Atmos. Meas. Tech. Discuss., 6, 3367–3405, 2013
www.atmos-meas-tech-discuss.net/6/3367/2013/
doi:10.5194/amtd-6-3367-2013

Atmospheric Measurement Techniques Discussions

McClear: a new model estimating downwelling solar radiation at ground level in clear-sky conditions

M. Lefèvre[1], A. Oumbe[1,2], P. Blanc[1], B. Espinar[1], B. Gschwind[1], Z. Qu[1], L. Wald[1], M. Schroedter-Homscheidt[2], C. Hoyer-Klick[2], A. Arola[3], A. Benedetti[4], J. W. Kaiser[4,5,6], and J.-J. Morcrette[4]

[1]MINES ParisTech, CS10207, 06904 Sophia Antipolis, France
[2]German Aerospace Center (DLR), Wessling, Germany
[3]Finnish Meteorological Institute, Kuopio, Finland
[4]ECMWF, Reading, UK
[5]King's College London, London, UK
[6]Max Planck Institute for Chemistry, Mainz, Germany

Received: 30 January 2013 – Accepted: 18 March 2013 – Published: 10 April 2013

Correspondence to: L. Wald (lucien.wald@mines-paristech.fr)

Published by Copernicus Publications on behalf of the European Geosciences Union.

Abstract

A new fast clear-sky model called McClear was developed to estimate the downwelling shortwave direct and global irradiances received at ground level under clear skies. McClear implements a fully physical modelling replacing empirical relations or simpler models used before. It exploits the recent results on aerosol properties, and total column content in water vapor and ozone produced by the MACC project (Monitoring Atmosphere Composition and Climate). It accurately reproduces the irradiance computed by the libRadtran reference radiative transfer model with a computational speed approximately 10^5 times greater by adopting the abaci, or look-up tables, approach combined with interpolation functions. It is therefore suited for geostationary satellite retrievals or numerical weather prediction schemes with many pixels or grid points, respectively. McClear irradiances were compared to 1 min measurements made in clear-sky conditions in several stations within the Baseline Surface Radiation Network in various climates. For global, respectively direct, irradiance, the correlation coefficient ranges between 0.95 and 0.99, resp. 0.86 and 0.99. The bias is comprised between -14 and $25\,W\,m^{-2}$, resp. -49 and $+33\,W\,m^{-2}$. The RMSE ranges between $20\,W\,m^{-2}$ (3 % of the mean observed irradiance) and $36\,W\,m^{-2}$ (5 %), resp. $33\,W\,m^{-2}$ (5 %) and $64\,W\,m^{-2}$ (10 %). These results are much better than those from state-of-the-art models. This work demonstrates the quality of the McClear model combined with MACC products, and indirectly the quality of the aerosol properties modeled by the MACC reanalysis.

1 Introduction

The downwelling solar irradiance observed at ground level on horizontal surfaces and integrated over the whole spectrum (total irradiance), is called surface solar irradiance (SSI). It is the sum of the direct irradiance, from the direction of the sun, and the diffuse, from the rest of the sky vault, and is also called the global irradiance. The SSI is

AMTD
6, 3367–3405, 2013

an Essential Climate Variable (ECV) as established by the Global Climate Observing System in August 2010 (GCOS, 2010). Knowledge of the SSI and its geographical distribution is of prime importance for numerous domains where SSI plays a major role as e.g. weather, climate, biomass, and energy.

Accurate assessments of SSI can be retrieved from satellite data and several studies demonstrate the superiority of satellite data over interpolation methods applied to sparse measurements performed within a radiometric network (Perez et al., 1997; Zelenka et al., 1999). Satellites are also a suitable supplement to rare long-term SSI measurements (Ba et al., 2001; Blanc et al., 2010; Cano et al., 1986; Darnell et al., 1996; Diabaté et al., 1988; Elias and Roujean, 2008; Lefèvre et al., 2007; Posselt et al., 2012; Raschke et al., 1987; Schiffer and Rossow, 1985; Schmetz, 1989).

The clear-sky model describes the SSI in a cloud-free atmosphere. It sets the upper limit of the SSI (Gueymard, 2012; Long and Ackerman, 2000). In many methods for the assessment of the SSI, all-sky irradiance is derived from the modelled clear-sky SSI by the attenuation or a modification factor due to clouds (Cano et al., 1986; Posselt et al., 2012; Raschke et al., 1987; Rigollier et al., 2004). While the all-sky SSI changes mainly with clouds, the SSI under clear-sky is strongly dependent on the composition of the atmosphere, namely the variable parameters aerosol and water vapour. Aerosols play a major role due to the diversity in scattering and absorbing properties according to their type, and the spatial and temporal heterogeneity of their number, size, chemical composition, and shape (Deepshikha et al., 2006; Deneke et al., 2008; Elias and Roujean, 2008; Gueymard, 2005; Xu et al., 2011).

The MACC project (Monitoring Atmosphere Composition and Climate) funded by the European Commission, is preparing the operational provision of global aerosol properties forecasts together with physically consistent total column content in water vapor and ozone (Kaiser et al., 2012a; Peuch et al., 2009). Up to now a multi-annual reanalysis dataset is provided and used here (Inness et al., 2012). Such information has not been available so far from any operational NWP centre.

AMTD
6, 3367–3405, 2013

A new clear-sky model called McClear is developed to exploit this new input data source for estimating the downwelling shortwave direct and global irradiances received at ground level. The aim of this article is to describe this model (Sect. 2), its implementation (Sect. 3), and to establish its performances (Sects. 4 and 5) with respect to high-quality measurements of SSI and published similar works (Sect. 6).

2 The McClear model

Let denote E^{diff} the diffuse irradiance on the horizontal plane, E^{dir} the direct (or beam) irradiance on the horizontal plane, and E^{glo} the global irradiance:

$$E^{\mathrm{glo}} = \left(E^{\mathrm{diff}} + E^{\mathrm{dir}}\right). \quad (1)$$

If *E0* denotes the irradiance that is received on a horizontal surface at the top of atmosphere for the location and time under concern, the clearness index *KT* is defined:

$$KT = E^{\mathrm{glo}}/E0. \quad (2)$$

The clearness index is also called global transmissivity of the atmosphere, or atmospheric transmitance, or atmospheric transmission. In the same way, we define the direct clearness index KT^{dir}:

$$KT^{\mathrm{dir}} = E^{\mathrm{dir}}/E0. \quad (3)$$

The model McClear aims at producing both E^{glo} and E^{dir}. The first constraint put in its development is that it should sufficiently accurately reproduce the SSI estimated by accurate radiative transfer models (RTM). The RTM libRadtran (Mayer and Kylling, 2005; Mayer et al., 2010) is taken here as a reference. The deviations between McClear and libRadtran outputs must obey constraints similar to those for radiation measurements

AMTD
6, 3367–3405, 2013

(WMO 2008): the bias shall be less than 3 W m^{-2} and 95 % of the differences should be less than 20 W m^{-2}.

The major constraint is that it should deliver time-series of irradiance, e.g. 15 min values over a year, much faster than libRadtran. The computational speed should be approximately 10^5 times greater in order to enable routine production in real time forecasting systems.

One solution to obey these constraints is to adopt the abaci approach combined with interpolation functions. The use of abaci – also called look-up tables (LUT) – is not new in this domain (Deneke et al., 2008; Huang et al., 2011; Mueller et al., 2009; Schulz et al., 2009). It reveals an efficient and fast means to provide estimates of values otherwise available from complex and slow models. One drawback is the resources and time needed to compute the abaci that may amount to months. Another drawback is that the abaci formulation has to be adapted to the available input data source. Therefore, this paper deals with the specifics of an abaci approach for typical numerical weather prediction output characteristics as represented in the MACC reanalysis dataset.

A set of abaci and interpolation functions to speed up the resolution of the radiative transfer equations is designed, developed and implemented. This ensemble of abaci and interpolation functions as well as functions to exploit them for aggregation in time and computation of the sun position is the model McClear.

Inputs to MCClear are 10 parameters describing the optical state of the atmosphere and the ground albedo:

- total column content in ozone and water vapour,
- standard atmospheric profile (see Sect. 3.2),
- aerosol optical depth (AOD) at 550 nm, Angstrom coefficient, and aerosol type: urban, continental clean, continental polluted, continental average, maritime clean, maritime polluted, maritime tropical, antarctic, and desert (see Sect. 3.4),
- altitude of site and elevation above the ground,

AMTD
6, 3367–3405, 2013

– ground albedo,

and other parameters describing the geographical location and the time:

– latitude, longitude and elevation above mean sea level (a.s.l.) of the site of interest,

– period of time requested,

– summarization period, i.e. period of integration of the radiation: 1 min, 15 min, 1 h, 1 d,

– time sampling step, usually identical to the summarization period.

Aerosols are described by standard aerosol types instead of using modelled AOD at different wavelengths explicitely. At the first glance this can be critizised as making no use of available additional aerosol type information available and it creates the need of a transition matrix from MACC output to aerosol type (see Sect. 3.4). However, it enhances the flexibility of the McClear use for other future sources of input data using other internal aerosol models and/or other output wavelengths. Additionally, it avoids the increase of the abaci dimensions in order to cover all AOD wavelengths and the shift for spectral interpolation assumptions from the AOD level on the irradiance level afterwards in the broadband irradiance generation.

The abaci contain:

– the clearness index KT for ground albedo equal to 0, 0.1, and 0.9 (see Sect. 3.1),

– the direct clearness index KT^{dir} for null ground albedo,

for selected values of the 10 inputs of McClear describing the optical state of the atmosphere and ground albedo. These values are called node points. The clearness indices are obtained by running libRadtran for these node points. Interpolation functions permit to interpolate between node points.

An optimization was made for the selection of the node points and interpolation functions with the following constraints: (i) decrease as much as possible the number of

AMTD
6, 3367–3405, 2013

node points, in order to have abaci as small as possible, (ii) select/design interpolation functions as fast as possible, and (iii) interpolated values must be close to the libRadtran results with already mentioned constraints. The last constraints on the difference with libRadtran were checked for each input separately as well as combination of all inputs using all node points and interpolation functions.

The optimization was done for each of the 10 inputs listed above. Using a Monte-Carlo technique, randomly selected sets of input to libRadtran are generated, with the exception of the current parameter which is regularly sampled with a small step. The random selection of the inputs is weighted by considering the average distribution in optical properties of the atmosphere. The probability density functions for all parameters, except aerosol optical thickness and Angstrom coefficient, and total column ozone, obey the uniform law. The chi-square law for aerosol optical thickness, the normal law for the Angstrom coefficient, and the beta law for total column ozone have been selected. The parameters of the laws have been empirically determined from various sources, such as scientific literature, re-analyses, AERONET data, and archives of ozone products of the spatial missions OMI, GOME and SCHIAMACHY.

For all inputs, the selected interpolation functions are linear interpolators, except for the solar zenithal angle Θ_S. For the latter, the modified Beer-Lambert (MLB) function proposed by Mueller et al. (2009) has been studied. To obey the constraints, a 5-piecewise MLB was retained with the following angles: 0°, 60°, 75°, 80°, 85°, 89.9° instead of the originally proposed two angles 0 and 60°. Shortly after the design of the abaci has been frozen, Qu et al. (2011) demonstrated that a 4-piecewise MLB with the angles: 0°, 60°, 75°, 85°, 89.9° would have been applicable as well.

Following Oumbe et al. (2011), the efficiency and accuracy of piecewise linear functions to estimate changes in E^{glo} and E^{dir} with altitude above the ground is sufficient.

The formula of Vermote et al. (1994, 1997) is used for the ground albedo ρ_g:

$$KT(\rho_g) = KT(\rho_g = 0)/(1 - \rho_g S) \quad (4)$$

AMTD
6, 3367–3405, 2013

where S is the unknown atmospheric spherical albedo. S is computed for $\rho_g = 0.1$, and 0.9 using Eq. (5), and then is linearly interpolated/extrapolated:

$$a = \left[S\left(\rho_g = 0.9\right) - S\left(\rho_g = 0.1\right)\right]/0.8 \quad (5)$$
$$b = S\left(\rho_g = 0.1\right) - 0.1\,a$$
$$S\left(\rho_g\right) = a\rho_g + b.$$

In total, this design results in 1674 abaci. One abacus corresponds to a given atmospheric profile and a given type of aerosol. In an abacus, the list of node points is:

- total column content in ozone (in Dobson unit): 200, 300, 400, 500,
- total column content in water vapour ($kg\,m^{-2}$): 0.1, 3, 5, 7, 10, 15, 20, 30, 40, 60, 80, 100,
- aerosol optical depth at 550 nm: 0.01, 0.05, 0.1, 0.2, 0.3, 0.5, 1, 1.5, 2, 5,
- aerosol Angstrom coefficient: −1, −0.5, 0, 0.5, 1, 1.5, 2, 3, 4,
- site elevation above mean sea level (km): 0, 1, 2, 3, 4, 5, 6, 7,
- elevation above ground level (km): 0, 0.5, 1, 1.5, 2,
- solar zenithal angle (deg): 0, 60, 75, 80, 85, 89.9.

3 Practical implementation of McClear

McClear can be run with self-defined inputs. More interestingly, it is capable of ingesting atmospheric data from the MACC modelling and from the MODIS (Moderate Resolution Imaging Spectroradiometer) estimates for ground albedo. This section details the practical implementation of McClear.

AMTD
6, 3367–3405, 2013

3.1 Ground albedo

The MCD43C2 data, derived from MODIS images, are 16-day composites provided as a level-3 product projected to a 0.05° grid in latitude/longitude. They are produced every 8 days with 16 days of acquisition, where the given date is that of the first day of the 16-days period. Three parameters are given describing the bidirectional reflectance distribution function (BRDF), from which the directional hemispherical reflectance (DHR) also called black-sky albedo and the bihemispherical reflectance (BHR) also called white-sky albedo (e.g. Schaepman-Strub et al., 2006) are computed. Defining $K^{\mathrm{dir}}(\rho_{\mathrm{g}})$ as:

$$K^{\mathrm{dir}}\left(\rho_{\mathrm{g}}\right) = E^{\mathrm{dir}}/E^{\mathrm{glo}}\left(\rho_{\mathrm{g}}\right) \tag{6}$$

where E^{dir} does not depend on ρ_{g}, the ground albedo ρ_{g} is given by:

$$\rho_{\mathrm{g}} = \mathrm{BHR} + K^{\mathrm{dir}}\left(\rho_{\mathrm{g}}\right)(\mathrm{DHR} - \mathrm{BHR}). \tag{7}$$

The major difficulty in Eq. (7) is that ρ_{g} depends upon K^{dir}, which depends itself on ρ_{g}. By combining Eqs. (4)–(7), and denoting $\Delta = (\mathrm{DHR} - \mathrm{BHR})$, one obtains a second-order equation in KT which is the quantity of interest:

$$a\Delta^2 KT^{\mathrm{dir}^2} + KT\left[KT\left(\rho_{\mathrm{g}} = 0\right) + (2a\,\mathrm{BHR} + b)\,\Delta\,KT^{\mathrm{dir}}\right] + (a\,\mathrm{BHR}^2 + b\,\mathrm{BHR} - 1)\,KT^2 = 0. \tag{8}$$

Using the Monte-Carlo technique to randomly select 100 000 samples, it is found that Eq. (8) has only one solution that respects $KT > KT^{\mathrm{dir}}$. Therefore, Eq. (8) is used to compute KT and Eq. (7) provides ρ_{g}.

In a practical manner, once a request is made for a given site, the three BRDF parameters are taken from the closest MCD43C2 grid point, and for the previous, current and following months for the current day. They are interpolated in time for each minute of the day, taking into account the possible absence of data. Then, Eq. (8) is solved for KT. As for the ocean, the first BRDF parameter is set to 0.02 (Wald and Monget, 1983) and the two others to 0.

AMTD
6, 3367–3405, 2013

3.2 Atmospheric profile

The five atmospheric profiles used in McClear are those from the USA Air Force Geophysics Laboratory (AFGL) as implemented in libRadtran: tropics, mid-latitude summer and winter, sub-artic summer and winter. A mask has been constructed for the automatic selection of the atmospheric profile for any site. The Koeppen climate classification map (FAO, 1997) has been manually modified for Northern America, China and Africa following Trewartha (1954). Other maps of climate classification could have been suitable and possibly more accurate. But aiming at partitioning the world in five classes only, a very limited level of details is sufficient. The subartic profiles are allotted to climate zones noted EF, ET, Dc, Dd in Trewartha (1954), the tropical profile to Aw, As, Af, and Am, and the mid-latitude profiles are allotted to the rest. Oceans are not covered by these climate maps; extension was manually made. As for the seasons, November to April is considered as boreal winter (austral summer).

3.3 Altitude correction

Inputs from MACC are given for a local mean elevation above mean sea level (a.s.l.). The mean MACC elevation for the site under concern is computed by linear interpolation of the 4 neighbors. Interpolation in clearness index is made between the two closest nodes "site elevation asl" in the abaci. If the actual elevation of the site is less than the mean MACC elevation, the clearness index is set to that corresponding to the mean elevation. Otherwise, an additional linear interpolation is performed using the nodes "elevation above ground level".

3.4 Aerosols properties

Inputs to McClear are the aerosol optical depth at 550 nm, Angstrom coefficient, and aerosol type. The MACC reanalysis delivers total aerosol optical depth at 550 and 1240 nm, from which the Angstrom coefficient is derived. It delivers also partial optical

AMTD
6, 3367–3405, 2013

depths at 550 nm for dust, organic, sea salt, sulphate, and black carbon aerosol species (Benedetti et al., 2009; Kaiser et al., 2012b; Morcrette et al., 2008, 2009).

These partial optical depths are used to automatically determine the aerosol type, and more exactly the mixture whose name describes the typical origin of the particle ensembles: urban, continental clean, continental polluted, continental average, maritime clean, maritime polluted, maritime tropical, antarctic, and desert. Table 1 in Holzer-Popp et al. (2002) gives percentage contributions to the total optical depth of the respective mixtures by the basic components: watersoluble, water insoluble, sea salt accumulation mode, coarse mode, soot, and mineral transported. It is used as a guide for converting MACC species into types. The partial optical depths are converted to fractions of the total optical depth, in percent. The conversion algorithm is described in Fig. 1. The type "antartic" is solely defined by the latitude.

The algorithm has been tested by running it over several years of MACC data. Several sites were selected for which one or more types were expected to dominate, such as sites in Indian and South Pacific Ocean (maritime tropical and maritime clean and polluted), North Atlantic Ocean (maritime, continental, and urban), Australian and Sahelian deserts (desert and continental), Tibet plateau and Amazonian forest (mostly continental, maritime), Zaire forest (continental, urban), large conurbations: Calcutta and New Delhi (urban, continental polluted), Beijing (urban), Shanghai and Mexico (urban, continental, maritime), Tamanrasset, Sede Boqer, and Mezaira (desert).

For each site, the histogram of the resulting types has been drawn and checked that it was close to our expectations. Though satisfactory as a whole, more work is needed on this algorithm, which may fail sometimes. Figure 2 exhibits E^{glo} measured at the station Carpentras every 1 min on 10 June 2006 and that estimated by McClear as an example of such a failure. This day was clear, except in the early morning before 07:00 UT. One can see that both curves agree perfectly; the aerosol type was found as "urban". There is an exception to the agreement from 08:00 to 11:30 UT where the type was found as "maritime polluted". This leads to an overestimation of E^{glo} with a peak of 30 W m^{-2}, from 998 W m^{-2} down to 968 W m^{-2}, i.e. 3 % of E^{glo} at 11:30 UT. At

AMTD
6, 3367–3405, 2013

this instant, E^{dir} amounts to 910 W m^{-2} and is unchanged as it does not depend upon the aerosol type.

3.5 Computing instantaneous clear-sky SSI for any site

Aerosol properties, and total column contents in water vapour and ozone in MACC are given every 3 h, starting at 00:00 UT. A bi-linear interpolation in space is applied to compute a time-series of 3 h values for the given location. A further interpolation in time is performed yielding time-series of these atmospheric quantities every 1 min in order to enable the production of 1 and 15 min SSI.

These 1 min values are inputs to the McClear model. The solar zenital angle is computed with the SG2 algorithm (Blanc and Wald, 2012) for the middle of the minute. An abacus is selected for the given atmospheric profile and aerosol type. A series of interpolations as described above is performed to yield the clearness indices. The ordering of interpolation of parameters was found as having a negligible influence on the results. For the sake of computing speed, linear interpolations are performed first, then the MLB interpolator, and finally the computation of the ground albedo.

The resulting clearness indices are assumed to be constant over 1 min. The 1 min mean irradiance is computed by Eqs. (2)–(3), where the solar geometry parameters and *E0* are determined by SG2 for the beginning and end of the minute. If requested, the 1 min irradiances are summarized to yield 15 min, hourly and daily values in Universal Time or True Solar Time.

4 BSRN data for validation

The Baseline Surface Radiation Network (BSRN) is a collection of measurements of E^{glo}, E^{diff} and beam normal irradiance (BNI) of high quality suitable for validation. Measurements are acquired every 1 min. Data sets were collected for 11 stations

AMTD
6, 3367–3405, 2013

representing a variety of climates (Table 1) for the period 2005–2008, except for Palaiseau, Xianghe and Lauder: 2005–2007, and Brasilia: 2006–2007.

The original data were filtered out using the algorithm by Roesch et al. (2011). Only data which obey the following constraints were kept:

$$\left(E^{\mathrm{diff}} + E^{\mathrm{dir}}\right)/E^{\mathrm{glo}} = 1 \pm 0.08 \quad \text{if } \Theta_S <= 75°$$
$$\left(E^{\mathrm{diff}} + E^{\mathrm{dir}}\right)/E^{\mathrm{glo}} = 1 \pm 0.15 \quad \text{if } \Theta_S > 75°. \tag{9}$$

A series of filters was applied on the results of Eq. (9) in order to retain reliable clear-sky instants. Firstly, only those minutes for which $E^{\mathrm{diff}}/E^{\mathrm{glo}}$ was less than 0.3, i.e. when the diffuse component is much less than the direct one, were retained. Secondly, a given instant t, expressed in min, was kept only if at least 30 % of the 1 min observations in the intervals $[t-90, t]$ and $[t, t+90]$ have been retained. Thirdly, the variability of the irradiance in this interval must not be too large in order to avoid cases of broken clouds. This test may also avoid noticeable spatial heterogeneity around the site if ergodicity is assumed. If m denotes the air mass computed from (Kasten and Young, 1989), a corrected clearness index, KT' (Ineichen and Perez, 1999) is computed:

$$KT' = KT/[1.031 \exp(-1.4/(0.9 + 9.4/m)) + 0.1]. \tag{10}$$

An instant was considered clear if the standard-deviation of KT' in the interval $[t-90, t+90]$ was less than a threshold, set empirically to 0.02. Only these 1 min clear-sky instants were retained for the validation. This algorithm has been compared to that proposed by Long and Ackerman (2000) which was found to be less restrictive.

5 Validation

The validation of McClear was made by comparing the aforementioned 1 min BSRN values for clear-sky and the McClear values calculated for these instants and the location of the site. Following the ISO standard (1995), we computed the deviations:

AMTD
6, 3367–3405, 2013

subtracting measurements for each instant from McClear estimations and summarizing these differences by the bias, the root mean square error (RMSE), and the squared correlation coefficient. We computed also the parameters of the least-squares fitting line. Relative values are expressed with respect to the mean observed value. This operation was performed for E^{glo} and E^{dir}, KT and KT^{dir}, site per site, all instants merged, and for different classes of E^{glo}, E^{dir}, KT, KT^{dir}, Θ_S, aerosol optical depth at 550 nm, aerosol Angstrom coefficient, aerosol type, atmospheric profile, total content in water vapor and ozone, ground albedo, year and month.

The following graphs illustrate the case of Payerne. Figures 3 and 4 are correlograms between measured and estimated E^{glo} and E^{dir}. We observe an overall good fit between estimates and observations: the points are well aligned along the 1 : 1 line with a small tendency towards overestimation with high E^{glo} and a limited scattering. The squared correlation coefficient is very large: 0.99 and 0.96, meaning that 99 % and 96 % of information contained in E^{glo} and E^{dir} is well explained by McClear. The relative bias is small: 4 % for E^{glo} and 1 % for E^{dir}, as well as the RMSE: 5 and 7 %. As expected, performances in E^{dir} are less than for E^{glo}; the effects of aerosols are more pronounced in beam than in global SSI. Cases of large deviations can be related to errors in estimation of the aerosol optical thickness. As a whole, there is a slight overestimation by McClear for both E^{glo} and E^{dir}.

Looking at details (not shown), the bias and RMSE are more or less constant as a function of E^{glo}, E^{dir}, or Θ_S. Aerosol types are mostly "maritime polluted" by far, then "urban", then "continental polluted"; the aerosol optical depth at 550 nm is mostly found between 0.01 and 0.30. No trend is observed in bias and RMSE as a function of these properties.

Figures 5 and 6 are correlograms between BSRN data and McClear estimates for the global and beam clearness indices. The changes in solar radiation at the top of the atmosphere due to changes in geometry, namely the daily course of the sun and seasonal effects, are usually well reproduced by models and lead to a de facto correlation between observations and estimates hiding potential weaknesses. Clearness

AMTD
6, 3367–3405, 2013

indices KT and KT^{dir} are stricter indicators of the performances of a model regarding its ability to estimate the optical state of the atmosphere. Also KT and KT^{dir} are not completely independent of Θ_S as they decrease as Θ_S increase but the dependency is much less pronounced than in SSI. In Figs. 5 and 6, KT and KT^{dir} exhibit lower squared correlation coefficient than E^{glo} and E^{dir}: 0.69 and 0.53, instead of 0.99 and 0.96.

In Fig. 5, the set of points is well aligned along the 1 : 1 line for KT with a slight overestimation as a whole. The relative bias and RMSE are 3 and 5 %, similar to those for E^{glo}.

As for KT^{dir} (Fig. 6), the set of points is more compact than for KT. The squared correlation coefficient is low: 0.53. Obviously, several changes in measured KT^{dir} cannot be reproduced by McClear. Nevertheless, the relative bias and RMSE are small: 1 and 8 %, very similar to those for E^{dir}.

Tables 2 and 3 report statistical quantities on the deviations between estimates and measurements in E^{glo} and E^{dir} for the 11 stations. Similar tables were constructed for KT and KT^{dir} (Tables 4 and 5).

The correlation coefficient in E^{glo} is very large ($r \geq 0.95$) for all stations (Table 2). The bias ranges between −14 and +25 W m^{-2}, i.e. less than 4 % of the mean observed value. Largest biases in relative value are found in Brasilia (Brazil), Payerne (Switzerland), and Carpentras (France). The slope of the fitting line is close to 1, between 0.96 and 1.04, except for Barrow (0.94). The RMSE ranges between 20 and 36 W m^{-2} and is less than 5 % of the mean observed value in all cases.

One should note that the statistical quantities slightly vary from one year to another. For example, the bias in E^{glo} for Payerne is 23 W m^{-2} in 2005, 17 W m^{-2} in 2006, 23 W m^{-2} in 2007, and 26 W m^{-2} in 2008. As a whole, we have observed no clear trend between these quantities and the year. There is no clear trend either with Θ_S, the aerosol properties and type, ground albedo, or content in ozone and water vapour. However, it appears that results are usually better for the summer months than for winter.

AMTD
6, 3367–3405, 2013

The correlation coefficient for E^{dir} (Table 3) is also very large ($r \geq 0.96$) for all stations except Xianghe ($r = 0.86$). The bias ranges between −49 and +33 W m^{-2}, and is less than 7 % of the mean observed value. Lowest biases in absolute values, less than 6 W m^{-2}, are found in Europe (Palaiseau, Carpentras, Payerne) and Australia (Alice-Springs), while largest values are found in Xianghe (China, −22 W m^{-2}), Sede Boquer (Israel, −49 W m^{-2}), Brasilia (+33 W m^{-2}), and Lauder (New Zealand, −33 W m^{-2}). The fitting line is close to the identity line with slopes ranging between 0.96 and 1.04, except for Xianghe (0.87) and Lauder (0.92). The RMSE is small in all cases and ranges from 35 and 68 W m^{-2}, i.e. less than 5 to 11 % of the observed means. Largest RMSE (≥ 50 W m^{-2}) are found for stations offering large bias (Xianghe, Sede Boqer, Brasilia, and Lauder). The good performances in E^{dir} are likely due to the accurate representation of aerosol properties and their change in time by the MACC data.

As a whole, we have observed no clear trend in performances with year, or Θ_S, aerosol properties and type, ground albedo, or content in ozone and water vapour. Similarly to E^{glo}, the statistical quantities vary slightly from one year to another. Results are usually better for the winter months than for summer, contrary to E^{glo}.

We have not taken into account the circumsolar irradiance to adjust E^{dir} estimated by McClear to ground measurements. Pyrheliometers have an aperture angle of 5°, and therefore include part of the circumsolar radiation into the measured E^{dir}. This circumsolar irradiance under clear-sky is less than 10 W m^{-2} (Oumbe et al., 2012); it may partly explain the bias in case of underestimation.

The diffuse component E^{diff} is computed by subtracting E^{dir} from E^{glo}. Therefore, the bias in E^{diff} can be computed from Tables 2 and 3. It ranges from −8 to 60 W m^{-2}. As a whole, E^{diff} is overestimated, except for Brasilia and Tamanrasset.

The squared correlation coefficient for the clearness index KT is less than for E^{glo} (Table 4). It is close to, or greater than 0.7, which means that 70 % or more of the 1 min changes observed in KT is well explained by McClear. Xianghe (39 %), Tateno (45 %)

AMTD
6, 3367–3405, 2013

and Sede Boquer (56 %) are exceptions. The bias ranges from −0.028 (−4 %) to 0.023 (3 %). The relative RMSE is comprised between 3 and 6 % of the mean observed value.

The squared correlation coefficient for the beam clearness index KT^{dir} is less than for E^{dir} (Table 5). Approximately between 50 and 75 % of the 1 min changes observed in KT^{dir} is explained by McClear, except for Xianghe (30 %), and Tateno (44 %). The bias ranges from −0.053 (Sede Boquer, −8 %) to 0.029 (Brasilia, +5 %). The relative RMSE is comprised between 6 and 11 % of the mean observed value.

One may note that the stations: Carpentras, Payerne, Xianghe, Tateno, and Lauder, have elevations asl below the mean MACC elevation (Table 1). No further elevation correction is applied in these cases; the elevation used for computation is the mean MACC elevation. Consequently, one may expect an overestimation of the direct component because of the theoretical underestimation of the air mass. This is not what is observed; over these 5 cases, 4 exhibit underestimation. For the time being, this effect is unnoticeable compared to remaining uncertainties in aerosol modelling as input data source.

6 Comparison with other modelled clear-sky values

Several models for assessing the SSI under clear-sky can be found in literature. They are usually validated against ground measurements as done in the present work but with a noticeable difference: inputs are atmospheric parameters taken from collocated measuring instruments. Hence these validations qualify the intrinsic performances of the model rather that its real-life performances (Gueymard, 2012; Ineichen, 2006; Mueller et al., 2004; Rigollier et al., 2000).

Schillings et al. (2003) have performed validation of their model against hourly irradiance received on a plane normal to the sun rays for 8 sites in Saudi Arabia. Clear-sky instants are defined by the values of their model. Their results cannot be directly compared to ours which have been obtained for E^{dir} (horizontal surface). However, relative

AMTD
6, 3367–3405, 2013

RMSE can be compared: it ranges from 13 to 17 % in their case, and 7 % (Tamanrasset) and 9 % (Sede Boqer) in ours.

The SoDa web site (www.soda-is.org) provides SSI from the database HelioClim-3v3 (HC3v3, Blanc et al., 2010; Espinar et al., 2012). The HelioClim database derives from images of the Meteosat series of satellites using the Heliosat-2 method (Rigollier et al., 2004) and the ESRA clear-sky model (ESRA, 2000; Rigollier et al., 2000) modified by Geiger et al. (2002) with the climatology of the Linke turbidity factor from Remund et al. (2003) as inputs. The Linke turbidity factor is a convenient approximation to model the atmospheric absorption and scattering of the solar radiation under clear-sky. The climatology of Remund et al. (2003) comprises 12 maps, one per month, covering the world by cells of 5′ of arc angle in size. The SoDa Service is able to provide 1 min E^{glo} which is compared to that from BSRN for the clear-sky instants and the stations in the field-of-view of Meteosat: Palaiseau, Carpentras, Payerne, Sede Boqer, and Tamanrasset.

Tables 6 and 7 report bias, RMSE and squared correlation coefficient for on the one hand HC3v3 and McClear on the other hand. It appears clearly than figures of merit of McClear are much better than those of HC3v3. Knowing that HC3v3 is exploited by many companies and researchers in solar energy – approximately 2 millions of time-series of HC3v3 were supplied by the SoDa Service in 2011, – one may measure the strong interest of McClear in this community.

7 Conclusions

The new clear-sky model McClear exhibits very satisfactory results as a fast implementation of radiative transfer theory for the direct and global irradiance. The comparison between McClear estimates and measurements of global and beam SSI for 11 stations in the world shows that a large correlation is attained. For 1 min averages of global, respectively direct, irradiance, the correlation coefficient ranges between 0.95 and 0.99, resp. 0.84 and 0.99. The bias is contained between −14 and 25 W m^{-2}, resp. −49 and

AMTD
6, 3367–3405, 2013

+33 W m^{-2}. The RMSE ranges between 20 W m^{-2} (3 % of the mean observed irradiance) and 36 W m^{-2} (5 %), resp. 33 W m^{-2} (5 %) and 64 W m^{-2} (10 %). As a whole, 95 % of the deviations are less than approximately 50 W m^{-2} for global and 70 W m^{-2} for direct irradiance.

Comparaisons with state-of-the-art clear-sky models show that McClear surpasses them, especially regarding RMSE and correlation coefficient. These very good results demonstrate the quality of the McClear model and indirectly the quality of the aerosol properties modeled by the MACC reanalysis.

Several stations exhibit insufficiently great correlation coefficients in clearness indices. These are related to uncertainties in aerosol properties, and more efforts are necessary for a better modelling of the aerosols.

Performances are still far from WMO standards: bias less than 3 W m^{-2} and 95 % of the deviations less than 20 W m^{-2}. However, despite being of high quality, BSRN measurements are not absolute references. In addition, we are comparing here pinpoint measurements with estimates made using quantities describing the optical state of the atmosphere computed over large grid cells. Because of the natural variability of the SSI over areas of a few km^2 or greater, Zelenka et al. (1999) have shown that one may expect a relative RMSE ranging from 10 to 15 % for hourly values and greater for 1 min values due to the spatial and temporal mis-matching. We have found relative RMSEs ranging between 3 and 6 %, i.e. below this limit.

The novelty of the McClear model is the inclusion of variable aerosol optical properties, water vapour, and ozone with a high update frequency of 3 h compared to the previously used monthly climatologies in clear sky models. The large correlation coefficient and the low standard-deviation, computed from the RMSE and bias, demonstrate that McClear offers accurate estimates of changes in time of the SSI.

Since MACC provides also forecasts of the aerosol properties and ozone, and various meteorological services provide forecasts of water vapour from any NWP center, McClear can also be used for forecasting of clear-sky irradiances in future.

AMTD
6, 3367–3405, 2013

The McClear model with inputs from MACC and MODIS is available as a Web service, i.e. an application that can be invoked via the Web. It obeys the OGC (Open Geospatial Consortium) standard for Web processing services (WPS) (Percivall et al. 2011). An interface has been developed to launch McClear within a standard Web browser and to obtain time-series of global and beam SSI under clear-sky for a given point and a given period for the following summarizations: 1 min, 15 min, 1 h and 1 day. This interface can be launched via the catalog of products in the MACC Web site (www.gmes-atmosphere.eu).

Acknowledgements. The research leading to these results has received funding from the European Union's Seventh Framework Programme (FP7/2007-2013) under Grant Agreement no. 218793 (MACC project) and no. 283576 (MACC-II project). The authors thank all ground station operators of the BSRN network for their valuable measurements and the Alfred-Wegener Institute for hosting the BSRN website. The authors thank Laurent Saboret for his valuable help in setting up the McClear application on the Web.

References

Ba, M., Frouin, R., Nicholson, S., and Dedieu, G.: Satellite-derived surface radiation budget over the African continent, Part I: Estimation of downward solar irradiance and albedo, J. Climate, 14, 60–76, 2001.

Benedetti, A., Morcrette, J.-J., Boucher, O., Dethof, A., Engelen, R. J., Fisher, M., Flentje, H., Huneeus, N., Jones, L., Kaiser, J. W., Kinne, S., Manglold, A., Razinger, M., Simmons, A. J., and Suttie, M.: Aerosol analysis and forecast in the European Centre for Medium-Range Weather Forecasts Integrated Forecast System: 2. Data assimilation, J. Geophys. Res., 114, D13205, doi:10.1029/2008JD011115, 2009.

Blanc, P. and Wald, L.: The SG2 algorithm for a fast and accurate computation of the position of the Sun, Solar Energy, 86, 3072–3083, doi:10.1016/j.solener.2012.07.018, 2012.

Blanc, P., Gschwind, B., Lefèvre, M., and Wald, L.: The HelioClim project: Surface solar irradiance data for climate applications, Remote Sens., 3, 343–361, doi:10.3390/rs3020343, 2010.

AMTD
6, 3367–3405, 2013

Cano, D., Monget, J. M., Albuisson, M., Guillard, H., Regas, N., and Wald, L.: A method for the determination of the global solar radiation from meteorological satellites data, Solar Energy, 37, 31–39, 1986.

Darnell, W. L., Staylor, W. F., Ritchey, N. A., Gupta, S. K., and Wilber, A. C.: Surface radiation budget: A long-term global dataset of shortwave and longwave fluxes, EOS Trans. AGU, 27 February 1996.

Deepshikha, S., Satheesh, S. K., and Srinivasan, J.: Dust aerosols over India and adjacent continents retrieved using METEOSAT infrared radiance Part I: sources and regional distribution, Ann. Geophys., 24, 37–61, doi:10.5194/angeo-24-37-2006, 2006.

Deneke, H. M., Feijt, A. J., and Roebeling, R. A.: Estimating surface solar irradiance from Meteosat SEVIRI-derived cloud properties, Remote Sens. Environ., 12, 3131–3141, 2008.

Diabaté, L., Demarcq, H., Michaud-Regas, N., and Wald, L.: Estimating incident solar radiation at the surface from images of the Earth transmitted by geostationary satellites: the Heliosat Project, Int. J. Solar Energy, 5, 261–278, 1988.

Elias, T. and Roujean, J.-L.: Estimation of the aerosol radiative forcing at ground level, over land, and in cloudless atmosphere, from METEOSAT-7 observation: method and case study, Atmos. Chem. Phys., 8, 625–636, doi:10.5194/acp-8-625-2008, 2008.

Espinar, B., Wald, L., Blanc, P., Lefèvre, M., Gschwind, B., Ménard, L., Wey, E., Thomas, C., and Saboret, L.: HELIOCLIM-3: A near-real time and long-term surface solar irradiance database, Workshop on Remote Sensing Measurements for Renewable Energy, 22–23 May 2012, available at: http://hal-ensmp.archives-ouvertes.fr/docs/00/74/15/64/PDF/2012_COSTWIREHC3_extendedabstractv2.pdf, last access: 24 January 2013, Risoe, Denmark, 2012.

ESRA – European Solar Radiation Atlas: Fourth edition, includ. CD-ROM, edited by: Scharmer, K. and Greif, J., Scientific advisors: Dogniaux, R., Page, J. K., Authors: Wald, L., Albuisson, M., Czeplak, G., Bourges, B., Aguiar, R., Lund, H., Joukoff, A., Terzenbach, U., Beyer, H. G., and Borisenko, E. P., published for the Commission of the European Communities by Presses de l'Ecole, Ecole des Mines de Paris, Paris, France, 2000.

FAO: Koeppen climate classification map, available at: www.fao.org/sd/EIdirect/climate/EIsp0002.htm (last access: 21 December 2012), 1997.

GCOS – Global Climate Observing System Essential Climate Variables, available online: www.wmo.int/pages/prog/gcos/index.php?name=EssentialClimateVariables, last access: 16 November 2012.

AMTD
6, 3367–3405, 2013

Geiger, M., Diabaté, L., Ménard, L., and Wald, L.: A web service for controlling the quality of measurements of global solar irradiation, Solar Energy, 73, 475–480, 2000.
Gueymard, C.: Importance of atmospheric turbidity and associated uncertainties in solar radiation and luminous efficacy modelling, Energy, 30, 1603–1621, 2005.
Gueymard, C.: Clear-sky irradiance predictions for solar resource mapping and large-scale applications: Improved validation methodology and detailed performance analysis of 18 broadband radiative models, Solar Energy, 86, 2145–2169, doi:10.1016/j.solener.2011.11.011, 2012.
Holzer-Popp, T., Schroedter, M., and Gesell, G.: Retrieving aerosol optical depth and type in the boundary layer over land and ocean from simultaneous GOME spectrometer and ATSR-2 radiometer measurements, 1, Method description, J. Geophys. Res., 107, 4578, doi:10.1029/2001JD002013, 2002.
Huang, G. H., Ma, M. G., Liang, S. L., Liu, S. M., and Li, X.: A LUT-based approach to estimate surface solar irradiance by combining MODIS and MTSAT data, J. Geophys. Res.-Atmos., 116, D22201, doi:10.1029/2011JD016120, 2011.
Ineichen, P.: Comparison of eight clear sky broadband models against 16 independent data banks, Solar Energy, 80, 468–478, 2006.
Ineichen, P. and Perez, R.: Derivation of cloud index from geostationary satellites and application to the production of solar irradiance and daylight illuminance data, Theor. Appl. Climatol., 64, 119–130, 1999.
Inness, A., Baier, F., Benedetti, A., Bouarar, I., Chabrillat, S., Clark, H., Clerbaux, C., Coheur, P., Engelen, R. J., Errera, Q., Flemming, J., George, M., Granier, C., Hadji-Lazaro, J., Huijnen, V., Hurtmans, D., Jones, L., Kaiser, J. W., Kapsomenakis, J., Lefever, K., Leitão, J., Razinger, M., Richter, A., Schultz, M. G., Simmons, A. J., Suttie, M., Stein, O., Thépaut, J.-N., Thouret, V., Vrekoussis, M., Zerefos, C., and the MACC team: The MACC reanalysis: an 8-yr data set of atmospheric composition, Atmos. Chem. Phys. Discuss., 12, 31247–31347, doi:10.5194/acpd-12-31247-2012, 2012.
ISO Guide to the Expression of Uncertainty in Measurement: first edition, International Organization for Standardization, Geneva, Switzerland, 1995.
Kaiser, J. W., Peuch, V.-H., Benedetti, A., Boucher, O., Engelen, R. J., Holzer-Popp, T., Morcrette, J.-J., Wooster, M. J., and the MACC-II Management Board: The pre-operational GMES Atmospheric Service in MACC-II and its potential usage of Sentinel-3 observations, ESA Special Publication SP-708, Proceedings of the 3rd MERIS/(A)ATSR and OCLI-SLSTR

AMTD
6, 3367–3405, 2013

(Sentinel-3) Preparatory Workshop, held in ESA-ESRIN, 15–19 October 2012, Frascati, Italy, 2012a.
Kaiser, J. W., Heil, A., Andreae, M. O., Benedetti, A., Chubarova, N., Jones, L., Morcrette, J.-J., Razinger, M., Schultz, M. G., Suttie, M., and van der Werf, G. R.: Biomass burning emissions estimated with a global fire assimilation system based on observed fire radiative power, Biogeosciences, 9, 527–554, doi:10.5194/bg-9-527-2012, 2012b.
Kasten, F. and Young, A. T.: Revised optical air mass tables and approximation formula, Appl. Optics, 28, 4735–4738, 1989.
Lefèvre, M., Diabaté, L., and Wald, L.: Using reduced data sets ISCCP-B2 from the Meteosat satellites to assess surface solar irradiance, Solar Energy, 81, 240–253, 2007.
Long, C. N. and Ackerman, T. P.: Identification of clear skies from broadband pyranometer measurements and calculation of downwelling shortwave cloud effects, J. Geophys. Res., 105, 15609, doi:10.1029/2000JD900077, 2000.
Mayer, B. and Kylling, A.: Technical note: The libRadtran software package for radiative transfer calculations – description and examples of use, Atmos. Chem. Phys., 5, 1855–1877, doi:10.5194/acp-5-1855-2005, 2005.
Mayer, B., Kylling, A., Emde, C., Buras, R., and Hamann, U.: libRadtran: library for radiative transfer calculations, Edition 1.0 for libRadtran version 1.5-beta, http://www.libradtran.org (last access: 10 April 2013), 2 February 2010.
Morcrette, J.-J., Beljaars, A., Benedetti, A., Jones, L., and Boucher, O.; Sea-salt and dust aerosols in the ecmwf ifs model, Geophys. Res. Lett., 35, L24813, doi:10.1029/2008GL036041, 2008.
Morcrette, J.-J., Boucher, O., Jones, L., Salmond, D., Bechtold, P., Beljaars, A., Benedetti, A., Bonet, A., Kaiser, J. W., Razinger, M., Schulz, M., Serrar, S., Simmons, A. J., Sofiev, M., Suttie, M., Tompkins, A. M., and Untch, A.: Aerosol analysis and forecast in the European Centre for Medium-Range Weather Forecasts Integrated Forecast System: Forward modeling, J. Geophys. Res., 114, D06206, doi:10.1029/2008JD011235, 2009.
Mueller, R., Dagestad, K. F., Ineichen, P., Schroedter, M., Cros, S., Dumortier, D., Kuhlemann, R., Olseth, J. A., Piernavieja, G., Reise, C., Wald, L., and Heinnemann, D.: Rethinking satellite based solar irradiance modelling – The SOLIS clear sky module, Remote Sens. Environ., 91, 160–174, 2004.

AMTD
6, 3367–3405, 2013

Mueller, R., Matsoukas, C., Gratzki, A., Behr, H., and Hollmann, R.: The CM-SAF operational scheme for the satellite based retrieval of solar surface irradiance – a LUT based eigenvector hybrid approach, Remote Sens. Environ., 113, 1012–1024, doi:10.1016/j.rse.2009.01.012, 2009.

Oumbe, A., Blanc, P., Gschwind, B., Lefevre, M., Qu, Z., Schroedter-Homscheidt, M., and Wald, L.: Solar irradiance in clear atmosphere: study of parameterisations of change with altitude, Adv. Sci. Res., 6, 199–203, doi:10.5194/asr-6-199-2011, 2011.

Oumbe A., Qu, Z., Blanc, P., Bru, H., Lefèvre, M., and Wald, L.: Modeling circumsolar irradiance to adjust beam irradiances from radiative transfer models to measurements, EMS Annual Meeting 2012, 10–14 September 2012, Lodz, Poland, 2012.

Percivall, G., Ménard, L., Chung, L.-K., Nativi, S., and Pearlman, J.: Geo-processing in cyberinfrastructure: making the web an easy to use geospatial computational platform, in: Proceedings, 34th International Symposium on Remote Sensing of Environment, 10–15 April 2011, available at: www.isprs.org/proceedings/2011/ISRSE-34/211104015Final00671.pdf, last access: 29 December 2012, Sydney, Australia, 2011.

Perez, R., Seals, R., and Zelenka, A.: Comparing satellite remote sensing and ground network measurements for the production of site/time specific irradiance data, Solar Energy, 60, 89–96, 1997.

Peuch, V.-H., Rouil, L., Tarrason, L., and Elbern, H.: Towards European-scale Air Quality operational services for GMES Atmosphere, 9th EMS Annual Meeting, EMS2009-511, 9th European Conference on Applications of Meteorology (ECAM) Abstracts, held 28 September–2 October 2009, Toulouse, France, 2009.

Posselt, R., Mueller, R. W., Stöckli, R., and Trentmann, J.: Remote sensing of solar surface radiation for climate monitoring – the CM-SAF retrieval in international comparison, Remote Sens. Environ., 118, 186–198, 2012.

Qu, Z., Blanc, P., Lefèvre, M., Wald, L., and Oumbe, A.: Study of the MLB parameterisation for change in surface solar irradiance with sun zenith angle in clear sky, Adv. Sci. Res., 6, 233–236, doi:10.5194/asr-6-233-2011, 2011.

Raschke, E., Gratzki, A., and Rieland, M.: Estimates of global radiation at the ground from the reduced data sets of the International Satellite Cloud Climatology Project, J. Climate, 7, 205–213, 1987.

AMTD
6, 3367–3405, 2013

Remund, J., Wald, L., Lefèvre, M., Ranchin, T., and Page J.: Worldwide Linke turbidity information, CD-ROM published by International Solar Energy Society, Proceedings of ISES Solar World Congress, 16–19 June, Göteborg, Sweden, 2003.
Rigollier, C., Bauer, O., and Wald, L.: On the clear sky model of the 4th European Solar Radiation Atlas with respect to the Heliosat method, Solar Energy, 68, 33–48, 2000.
Rigollier, C., Lefèvre, M., and Wald, L.: The method Heliosat-2 for deriving shortwave solar radiation from satellite images, Solar Energy, 77, 159–169, 2004.
Roesch, A., Wild, M., Ohmura, A., Dutton, E. G., Long, C. N., and Zhang, T.: Assessment of BSRN radiation records for the computation of monthly means, Atmos. Meas. Tech., 4, 339–354, doi:10.5194/amt-4-339-2011, 2011.
Schaepman-Strub, G., Schaepman, M. E., Painter, T. H., Dangel, S., and Martonchik, J. V.: Reflectance quantities in optical remote sensing: Definitions and case studies, Remote Sens. Environ., 103, 27–42, 2006.
Schiffer, R. and Rossow, W. B.: ISCCP global radiance data set: A new resource for climate research, B. Am. Meteorol. Soc., 66, 1498–1503, 1985.
Schillings, C., Meyer, R., and Mannstein, H.: Validation of a method for deriving high resolution direct normal irradiance from satellite data and application for the Arabian Peninsula, Solar Energy, 76, 485–497, 2004.
Schmetz, J.: Towards a surface radiation climatology: retrieval of downward irradiances from satellites, Atmos. Res., 23, 287–321, 1989.
Schulz, J., Albert, P., Behr, H.-D., Caprion, D., Deneke, H., Dewitte, S., Dürr, B., Fuchs, P., Gratzki, A., Hechler, P., Hollmann, R., Johnston, S., Karlsson, K.-G., Manninen, T., Müller, R., Reuter, M., Riihelä, A., Roebeling, R., Selbach, N., Tetzlaff, A., Thomas, W., Werscheck, M., Wolters, E., and Zelenka, A.: Operational climate monitoring from space: the EUMETSAT Satellite Application Facility on Climate Monitoring (CM-SAF), Atmos. Chem. Phys., 9, 1687–1709, doi:10.5194/acp-9-1687-2009, 2009.
Trewartha, G. T.: An Introduction to Climate, 3rd Edn., McGraw Hill Book Co., 1954.
Vermote, E. F., Tanré, D., Deuzé, J. L., Herman, M., and Morcrette, J. J.: Second Simulation of the satellite signal in the solar spectrum (6S), 6S User Guide, NASA-Goddard Space Flight Center-Code 923, Greenbelt, USA, 1994.
Vermote, E. F., Tanré, D., Deuzé, J. L., Herman, M., and Morcrette, J. J.: Second simulation of the satellite signal in the solar spectrum: An overview, IEEE T. Geosci. Remote, 35, 675–686, 1997.

AMTD
6, 3367–3405, 2013

Wald, L. and Monget, J. M.: Remote sensing of the sea-state using the 0.8–1.1 microns channel (Comments by P. Koepke and reply, 6, 787–799, 1985), Int. J. Remote Sens., 4, 433–446, 1983.

WMO: Guide to meteorological instruments and methods of observation, World Meteorological Organization, WMO-No. 8, 7th Edn., Geneva, Switzerland, 2008.

Xu, J., Li, C., Shi, H., He, Q., and Pan, L.: Analysis on the impact of aerosol optical depth on surface solar radiation in the Shanghai megacity, China, Atmos. Chem. Phys., 11, 3281–3289, doi:10.5194/acp-11-3281-2011, 2011.

Zelenka, A., Perez, R., Seals, R., and Renné, D.: Effective accuracy of satellite-derived hourly irradiances, Theor. Appl. Climatol, 62, 199–207, 1999.

AMTD
6, 3367–3405, 2013

Table 1. List of BSRN stations used for validation.

Station	Code	Country	Latitude	Longitude	Elevation a.s.l. (m)	MACC mean altitude (m)
Barrow	BAR	USA-Alaska	71.323	−156.607	8	31
Palaiseau	PAL	France	48.713	2.208	156	126
Carpentras	CAR	France	44.083	5.059	100	538
Payerne	PAY	Switzerland	46.815	6.944	491	943
Xianghe	XIA	China	39.754	116.962	32	326
Tateno	TAT	Japan	36.050	140.133	25	246
Sede-Boqer	SBO	Israel	30.905	34.782	500	450
Tamanrasset	TAM	Algeria	22.780	5.510	1385	1012
Brasilia	BRB	Brazil	−15.601	−47.713	1023	808
Alice-Springs	ASP	Australia	−23.798	133.888	547	554
Lauder	LAU	New-Zealand	−45.045	+169.689	350	509

AMTD
6, 3367–3405, 2013

Table 2. Comparison between clear-sky global irradiances measured by BSRN and estimated by McClear.

Station	Number of samples	Mean observed value $W\,m^{-2}$	Bias $W\,m^{-2}$	Rel. bias %	RMSE $W\,m^{-2}$	Rel. RMSE %	Fitted straight line	Squared correl. coeff.
Barrow	70 283	498	−14	−3 %	27	5 %	$0.94\,x + 16$	0.98
Palaiseau	29 222	598	6	1 %	24	4 %	$1.03x - 9$	0.99
Carpentras	300 468	596	+20	+3 %	29	5 %	$1.04\,x$	0.99
Payerne	136 879	629	+22	+4 %	31	5 %	$1.02\,x + 9$	0.99
Xianghe	33 795	791	−7	−1 %	36	5 %	$0.98\,x + 7$	0.91
Tateno	133 433	590	+10	+2 %	28	5 %	$1.01\,x + 2$	0.98
Sede-Boqer	304 550	785	+11	+2 %	30	3 %	$0.96\,x + 40$	0.99
Tamanrasset	331 045	791	+7	+1 %	20	3 %	$0.96\,x + 37$	0.99
Brasilia	73 563	649	+25	+4 %	35	5 %	$1.02\,x + 13$	0.99
Alice-Springs	442 315	715	+12	+2 %	24	3 %	$1.00x + 11$	0.99
Lauder	117 090	600	+6	+1 %	21	4 %	$0.99\,x + 12$	0.99

AMTD
6, 3367–3405, 2013

Table 3. Comparison between clear-sky beam irradiances on horizontal surface measured by BSRN and estimated by McClear.

Station	Number of samples	Mean observed value $W\,m^{-2}$	Bias $W\,m^{-2}$	Rel. bias %	RMSE $W\,m^{-2}$	Rel. RMSE %	Fitted straight line	Squared correl. coeff.
Barrow	70 283	406	−21	−5 %	41	10 %	$0.96\,x - 4$	0.93
Palaiseau	29 222	492	−4	−1 %	37	7 %	$1.02\,x - 14$	0.96
Carpentras	300 468	505	−1	−0 %	35	7 %	$1.00\,x$	0.97
Payerne	136 879	530	+6	+1 %	39	7 %	$0.99\,x + 14$	0.97
Xianghe	33 795	643	−22	−3 %	64	10 %	$0.87\,x + 59$	0.74
Tateno	133 433	485	−16	−3 %	44	9 %	$1.04\,x - 38$	0.94
Sede-Boqer	304 550	667	−49	−7 %	63	9 %	$0.98\,x - 38$	0.95
Tamanrasset	331 045	653	+15	+2 %	48	7 %	$1.05\,x - 14$	0.95
Brasilia	73 563	560	+33	+6 %	48	9 %	$1.06\,x + 1$	0.98
Alice-Springs	442 315	634	+4	+1 %	33	5 %	$1.02\,x - 11$	0.98
Lauder	117 090	544	−33	−6 %	48	9 %	$0.92\,x + 3$	0.98

AMTD
6, 3367–3405, 2013

Table 4. Comparison between clear-sky global clearness indices measured by BSRN and estimated by McClear.

Station	Number of samples	Mean observed value	Bias	Rel. bias %	RMSE	Rel. RMSE %	Squared correl. coeff.
Barrow	70 283	0.76	−0.028	−4 %	0.043	6 %	0.71
Palaiseau	29 222	0.71	+0.002	+0 %	0.029	4 %	0.62
Carpentras	300 468	0.72	+0.023	+3 %	0.035	5 %	0.69
Payerne	136 879	0.73	+0.023	+3 %	0.036	5 %	0.69
Xianghe	33 795	0.75	−0.010	−1 %	0.037	5 %	0.39
Tateno	133 433	0.72	+0.019	+3 %	0.039	5 %	0.45
Sede-Boqer	304 550	0.75	+0.010	+1 %	0.032	4 %	0.56
Tamanrasset	331 045	0.79	+0.013	+2 %	0.027	4 %	0.71
Brasilia	73 563	0.74	+0.022	+3 %	0.032	4 %	0.74
Alice-Springs	442 315	0.77	+0.014	+2 %	0.024	3 %	0.82
Lauder	117 090	0.74	+0.015	+2 %	0.029	4 %	0.75

AMTD
6, 3367–3405, 2013

Table 5. Comparison between clear-sky beam clearness indices on horizontal surface measured by BSRN and estimated by McClear.

Station	Number of samples	Mean observed value	Bias	Rel. bias %	RMSE	Rel. RMSE %	Squared correl. coeff.
Barrow	70 283	0.61	−0.040	−6 %	0.066	11 %	0.55
Palaiseau	29 222	0.58	−0.011	−2 %	0.046	8 %	0.61
Carpentras	300 468	0.60	−0.004	−1 %	0.044	7 %	0.64
Payerne	136 879	0.61	+0.004	1 %	0.048	8 %	0.53
Xianghe	33 795	0.61	−0.023	−4 %	0.064	11 %	0.30
Tateno	133 433	0.59	−0.021	−4 %	0.057	10 %	0.44
Sede-Boqer	304 550	0.64	−0.053	−8 %	0.067	11 %	0.59
Tamanrasset	331 045	0.66	+0.014	+2 %	0.043	7 %	0.64
Brasilia	73 563	0.63	+0.029	+5 %	0.044	7 %	0.75
Alice-Springs	442 315	0.67	+0.002	+0 %	0.037	6 %	0.75
Lauder	117 090	0.66	−0.035	−5 %	0.054	8 %	0.72

AMTD
6, 3367–3405, 2013

Table 6. Comparison between clear-sky global irradiances on a horizontal surface measured by BSRN and estimated by HelioClim-3v3 (HC3v3) or by McClear.

Station		Number of samples	Mean observed value $W\,m^{-2}$	Bias $W\,m^{-2}$	Rel. bias %	RMSE $W\,m^{-2}$	Rel. RMSE %	Squared correl. coeff.
Palaiseau	HC3v3	28 292	598	−1	−0 %	62	10 %	0.97
	McClear	29 222	598	+6	+1 %	24	4 %	0.99
Carpentras	HC3v3	298 410	596	−11	−2 %	45	8 %	0.98
	McClear	300 468	596	+20	+3 %	29	5 %	0.99
Payerne	HC3v3	136 225	629	−43	−7 %	62	10 %	0.96
	McClear	136 879	629	+22	+4 %	31	5 %	0.99
Sede Boqer	HC3v3	303 869	784	−35	−4 %	54	7 %	0.96
	McClear	304 550	785	+11	+2 %	30	3 %	0.99
Tamanrasset	HC3v3	330 194	791	−24	−3 %	37	5 %	0.99
	McClear	331 045	791	+7	+1 %	20	3 %	0.99

AMTD
6, 3367–3405, 2013

Table 7. Comparison between clear-sky beam irradiances on a horizontal surface measured by BSRN and estimated by HelioClim-3v3 (HC3v3) or by McClear.

Station		Number of samples	Mean observed value $W\,m^{-2}$	Bias $W\,m^{-2}$	Rel. bias %	RMSE $W\,m^{-2}$	Rel. RMSE %	Squared correl. coeff.
Palaiseau	HC3v3	28 292	492	−14	−3 %	79	16 %	0.91
	McClear	29 222	492	−4	−1 %	37	7 %	0.96
Carpentras	HC3v3	298 410	505	−46	−9 %	76	15 %	0.93
	McClear	300 468	505	−1	−0 %	35	7 %	0.97
Payerne	HC3v3	136 225	530	−94	−18 %	111	21 %	0.90
	McClear	136 879	530	+6	+1 %	39	7 %	0.96
Sede Boqer	HC3v3	303 869	667	−89	−13 %	118	18	0.85
	McClear	304 550	667	−49	−7 %	63	9 %	0.95
Tamanrasset	HC3v3	330 194	653	−14	−2 %	87	13 %	0.86
	McClear	331 045	653	+15	+2 %	48	7 %	0.95

AMTD
6, 3367–3405, 2013

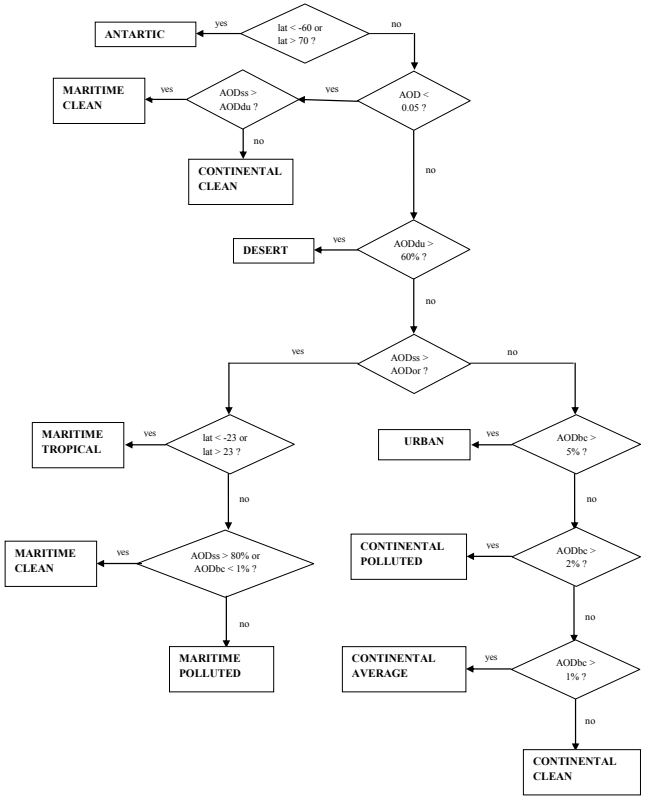

Fig. 1. Sketch of the algorithm converting the total optical depth (AOD) and partial optical depths of MACC species: dust (AODdu), sea salt (AODss), black carbon (AODbc), organic matter (AODor), into aerosol types: urban, continental clean, continental polluted, continental average, maritime clean, maritime polluted, maritime tropical, antarctic, and desert. "lat" is latitude.

AMTD
6, 3367–3405, 2013

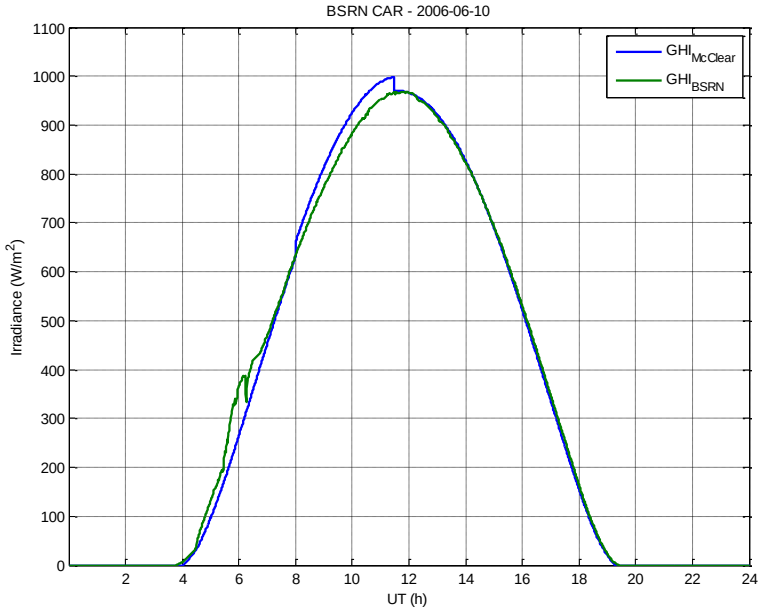

Fig. 2. Profiles of the 1 min global irradiance measured (BSRN) and estimated on 10 June 2006, at Carpentras, South-East of France as an example for a rare failure case of the aerosol type selection scheme.

AMTD
6, 3367–3405, 2013

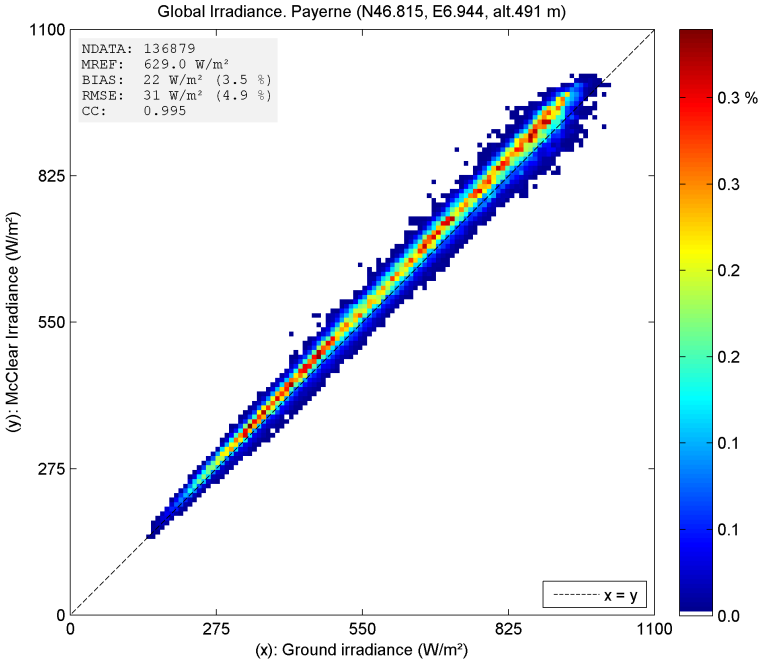

Fig. 3. Scatter density plot between BSRN 1 min clear-sky data and McClear. Payerne. Global irradiance on horizontal surface.

AMTD
6, 3367–3405, 2013

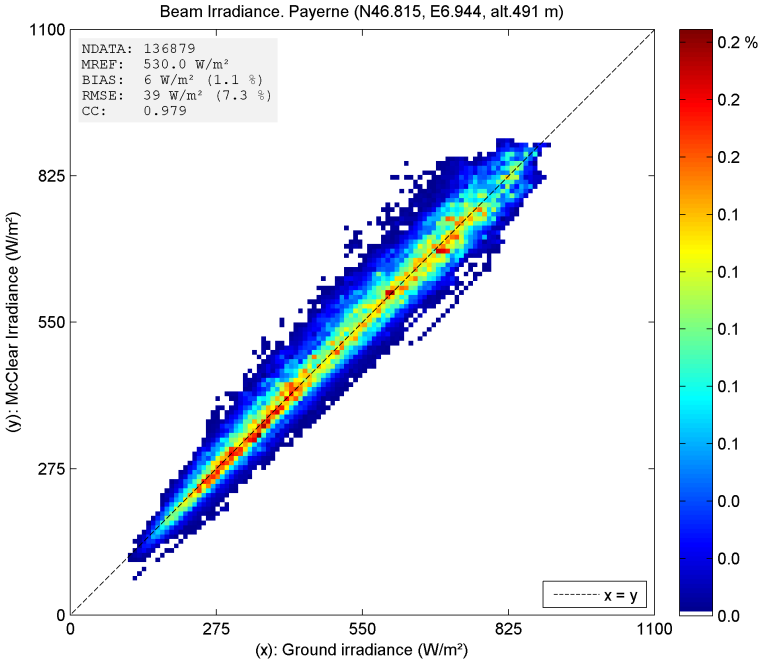

Fig. 4. Scatter density plot between BSRN 1 min clear-sky data and McClear. Payerne. Beam irradiance on horizontal surface.

AMTD
6, 3367–3405, 2013

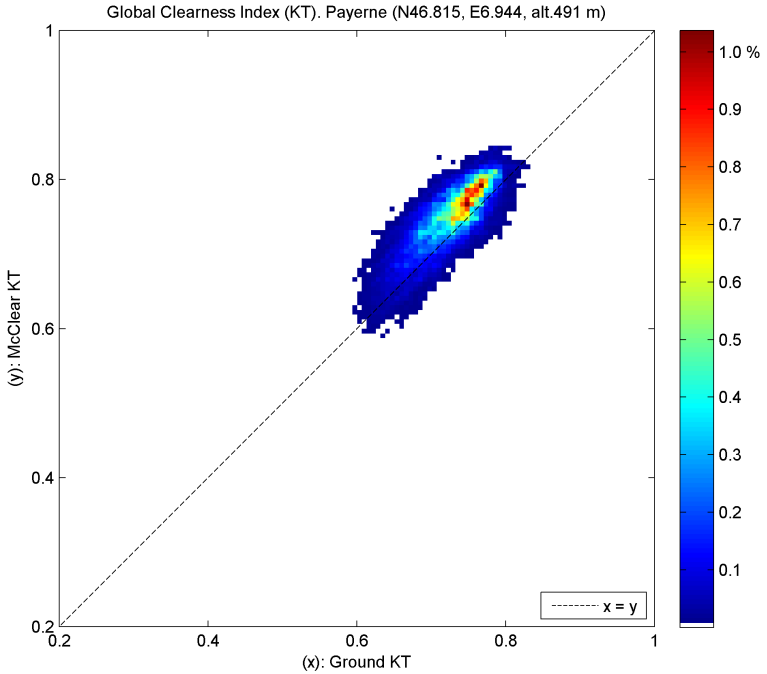

Fig. 5. Scatter density plot for 136 879 samples between BSRN 1 min clear-sky data and McClear. Payerne. Global clearness index *KT*.

AMTD
6, 3367–3405, 2013

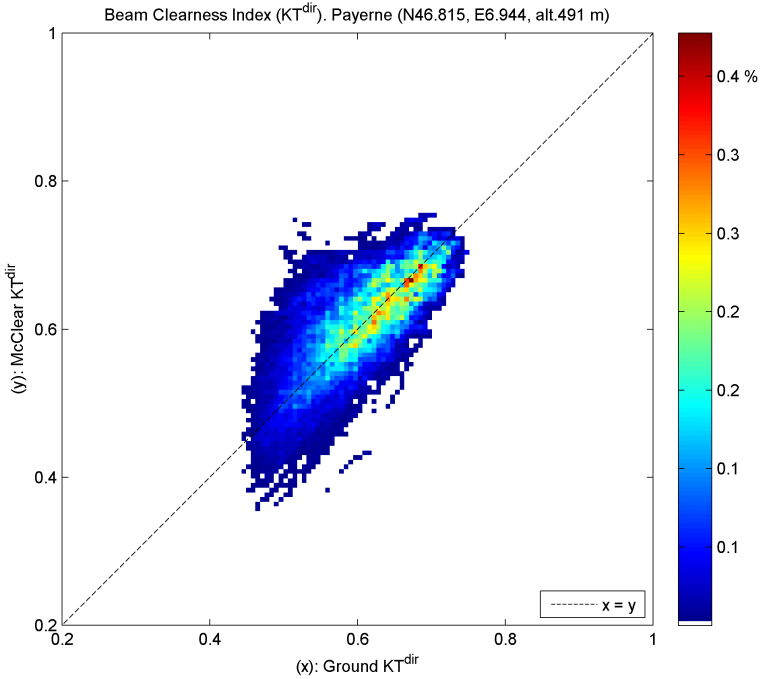

Fig. 6. Scatter density plot for 136 879 samples between BSRN 1 min clear-sky data and McClear. Payerne. Beam clearness index KT^{dir}.

AMTD
6, 3367–3405, 2013